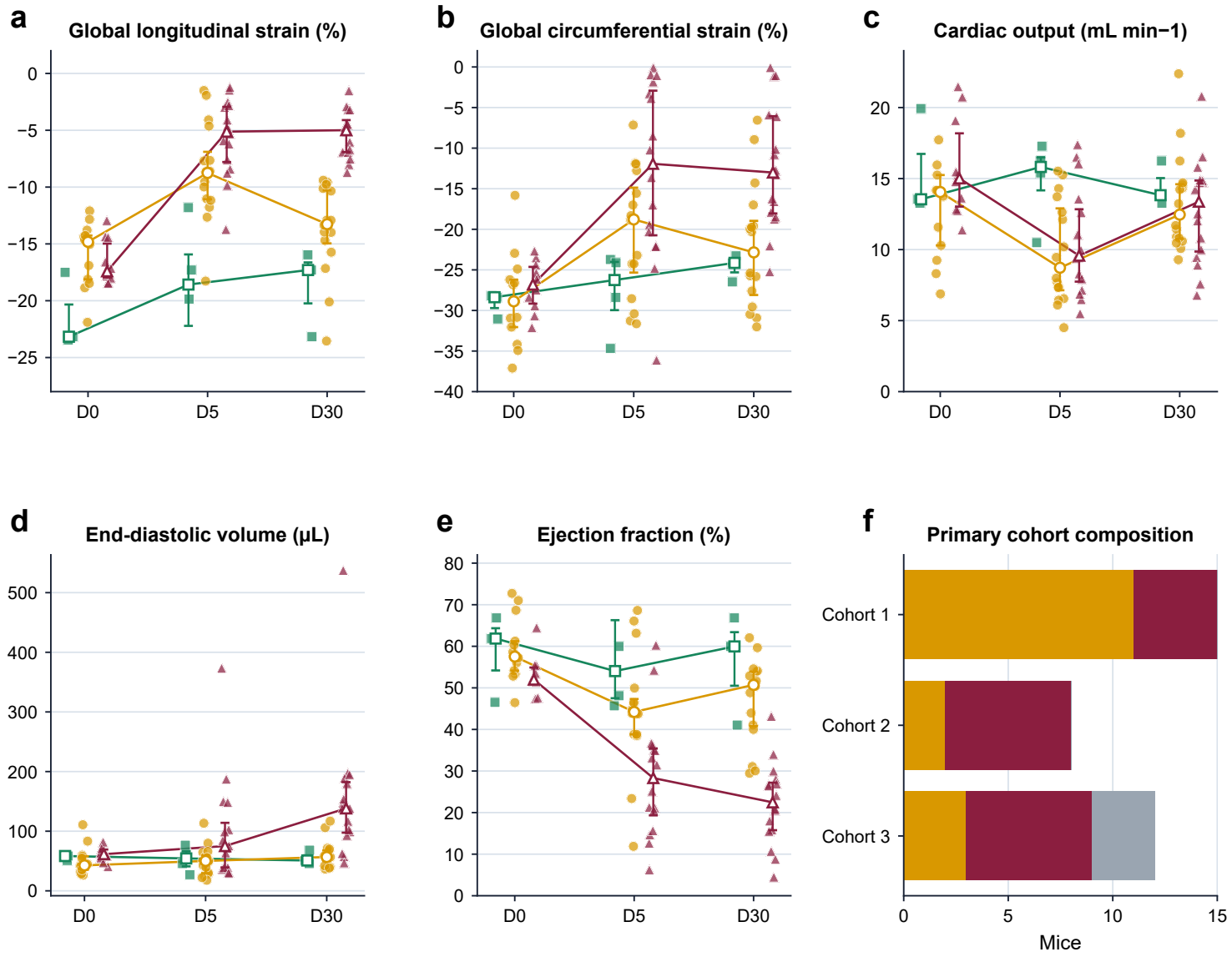
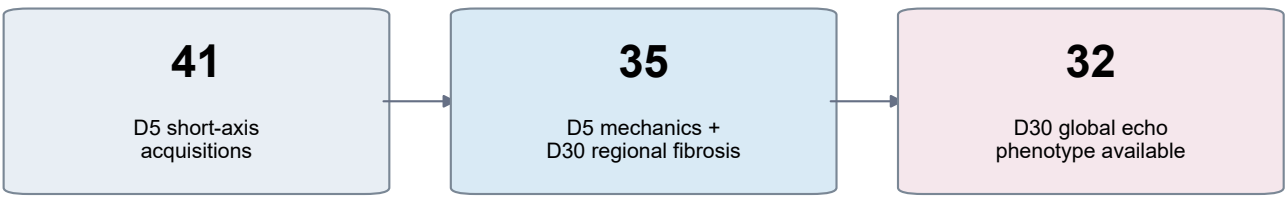
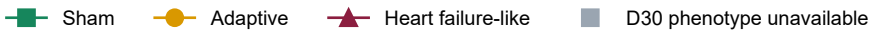


g



The 35-mouse prediction cohort was retained irrespective of D30 global phenotype availability.

h



Late remodeling phenotype: D30 GLS < −9% (adaptive) or ≥ −9% (heart failure-like)

Only mice with observed D30 GLS are shown in phenotype-stratified trajectories (16 per infarct group).

Sham animals are descriptive controls and were not included in adaptive versus heart failure-like comparisons.

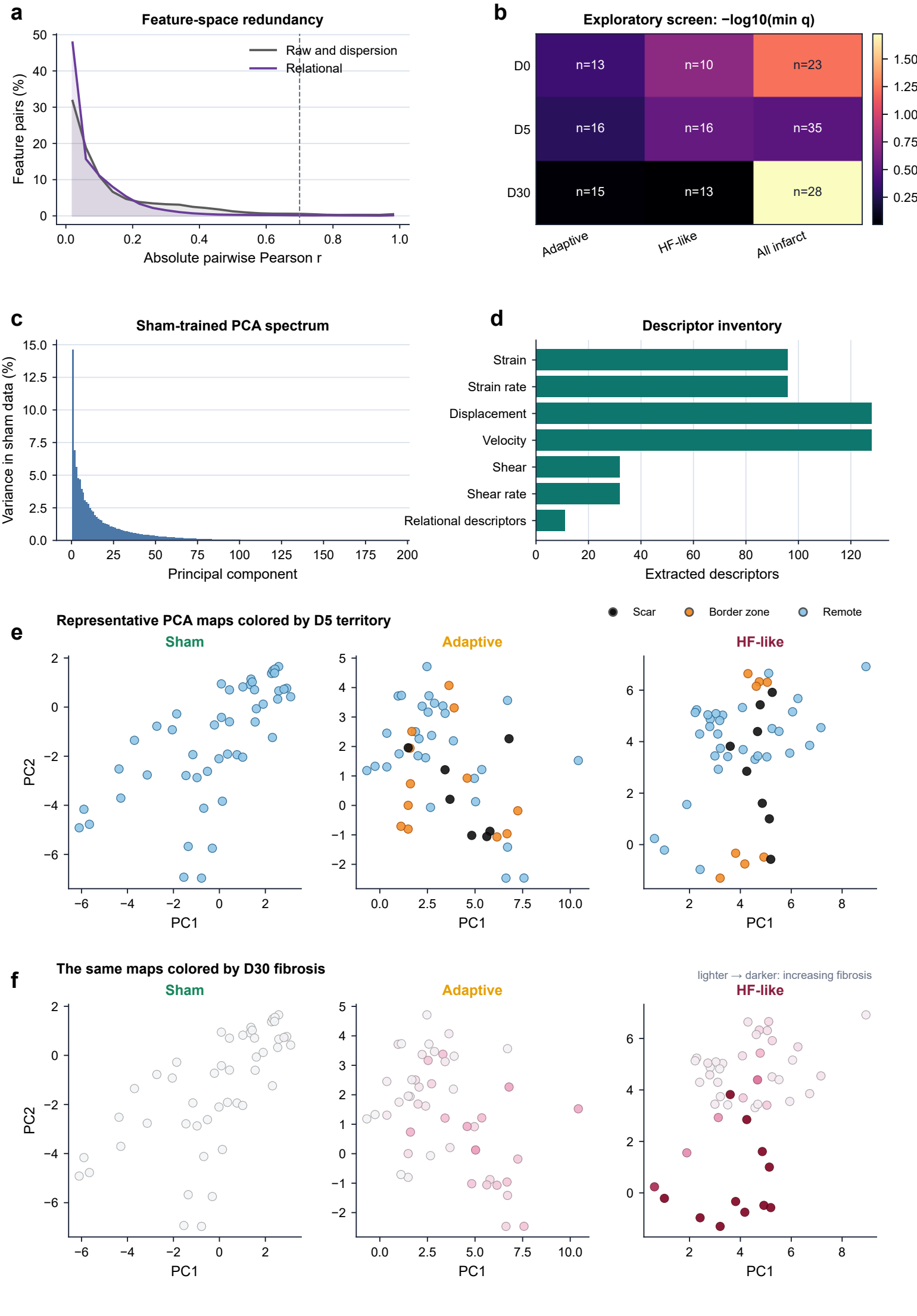
Supplementary Figure S1 | Global cardiac phenotype and analytical sample context.

a-e, Global longitudinal strain (GLS), global circumferential strain (GCS), cardiac output, end-diastolic volume and ejection fraction at baseline (D0), D5 and D30. Small filled symbols represent individual mice; larger open symbols and error bars indicate medians and interquartile ranges. Lines connect group medians, not individual trajectories. Infarcted mice were classified using observed D30 GLS: adaptive, GLS < -9%; heart failure-like, GLS >= -9% (16 mice per group). These D30 classifications were also used to group their earlier measurements. The four identified sham mice are descriptive controls. Available observations were used for each metric and time point; measurement availability is reported in the source data.

f, Composition of the 35-mouse primary cohort across three experiments (15, 8 and 12 mice, respectively). Three mice without D30 global echocardiography were not assigned a remodeling phenotype, but remained in fibrosis-prediction analyses.

g, Analytical sample flow. The imaging inventory contained 41 D5 short-axis acquisitions in addition to four identified sham controls; 35 mice had matched D5 regional mechanics and D30 regional fibrosis, and 32 of these had D30 global echocardiography. The six unmatched acquisitions lacked linked regional D30 fibrosis records in the analysis dataset. This inventory does not establish reasons for attrition or an operated-animal survival denominator.

h, Group and phenotype definitions. The mouse is the biological unit throughout this figure.


a
Feature-space redundancy
Raw and dispersion
Relational
Feature pairs (%)
Absolute pairwise Pearson r
b
Exploratory screen: −log10(min q)
D0
D5
D30
n=13
n=10
n=23
n=16
n=16
n=35
n=15
n=13
n=28
Adaptive
HF-like
All infarct
c
Sham-trained PCA spectrum
Variance in sham data (%)
Principal component
d
Descriptor inventory
Strain
Strain rate
Displacement
Velocity
Shear
Shear rate
Relational descriptors
Extracted descriptors
e
Representative PCA maps colored by D5 territory
Scar
Border zone
Remote
Sham
Adaptive
HF-like
PC1
PC2
f
The same maps colored by D30 fibrosis
lighter → darker: increasing fibrosis

Supplementary Figure S2 | Structure and exploratory assessment of summarized mechanical descriptors.

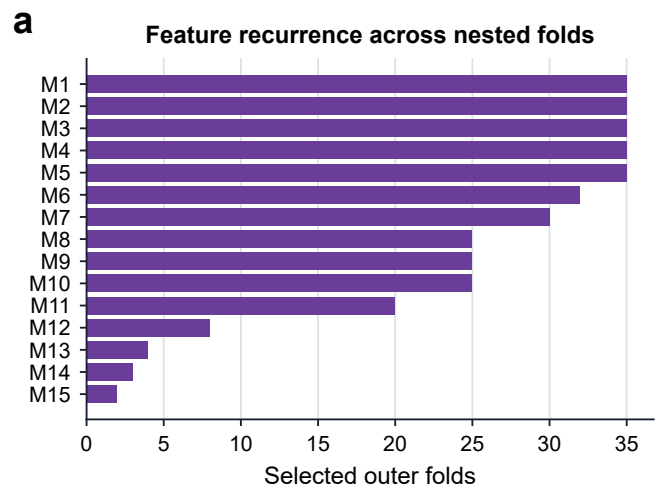
a, Distribution of absolute pairwise Pearson correlations among raw/dispersion descriptors and relational descriptors. Shading indicates the area under each frequency curve, not uncertainty; the dashed line marks |r| = 0.70.

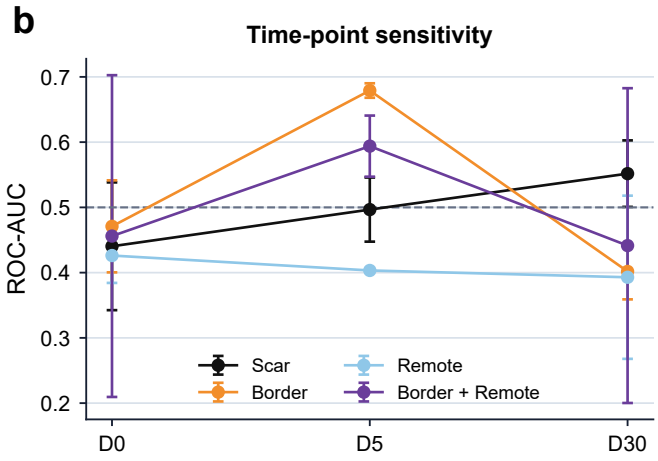
b, Exploratory associations between mouse-level mechanical summaries and mean continuous D30 whole-wall fibrosis percentages across all 48 sectors. Two-sided Pearson tests used the same 480 descriptors selected by mechanics-only collinearity refinement; Benjamini-Hochberg correction was applied separately within each time point and group across the valid descriptor tests. Color represents -log10 of the smallest q value in that family, not a prediction-performance measure. Subgroups use the verified D30 GLS classifications in Supplementary Fig. S1. Maximum complete-case sample sizes are 13 adaptive/10 heart failure-like/23 pooled at D0, 16/16/35 at D5 and 15/13/28 at D30. Labels in the heatmap show these maximum sample sizes; descriptor-specific counts can be lower because of missing measurements and are provided in the source tables. Three mice without D30 GLS contribute to the pooled D5 analysis only. This descriptive screen is distinct from the primary prediction of fibrosis burden outside scar and was not used to tune that model.

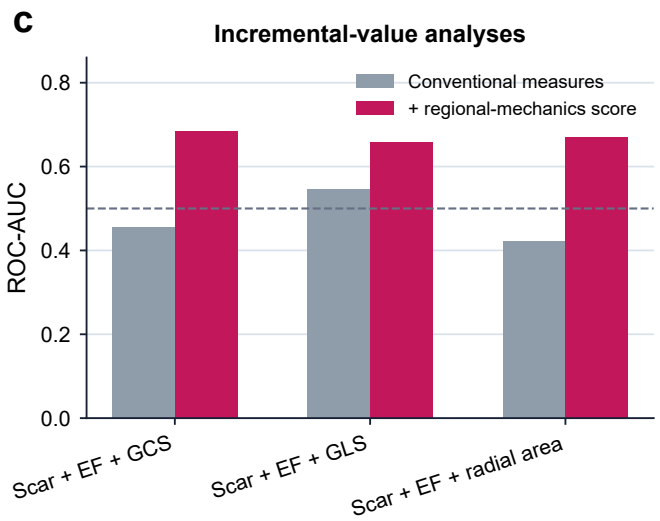
c, Explained-variance spectrum of the principal-component analysis (PCA) fitted using regional observations from four sham mice. The PCA is a visualization of the mechanical feature space, not a prediction model.

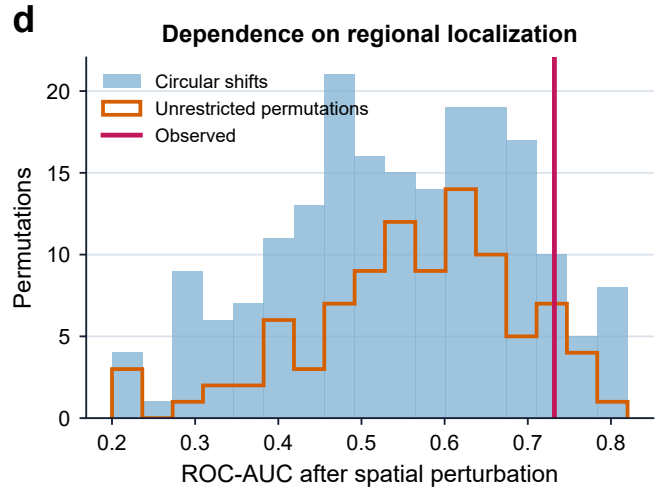
d, Descriptor counts by mechanical signal family.

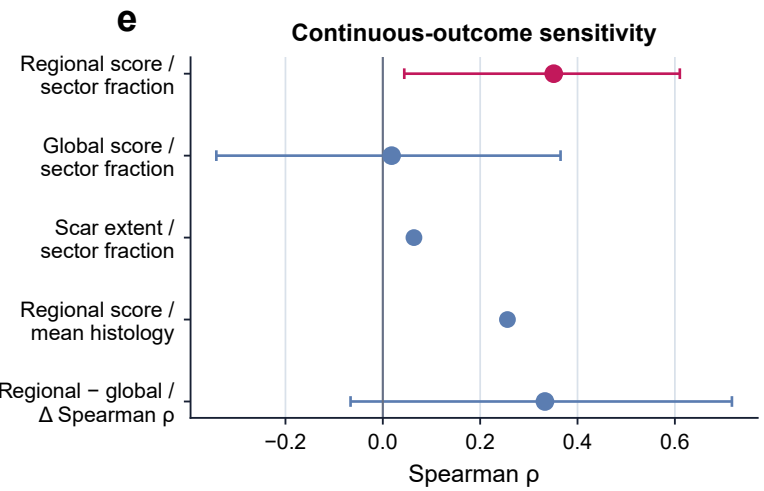
e,f, Identical PCA coordinates for representative sham, adaptive and heart failure-like mice, colored by D5 mechanical territory (e) or continuous D30 fibrosis percentage (f). Each point is a circumferential sector; sectors are nested within mice. Fibrosis was not used to fit the PCA. Panels c and d do not display uncertainty intervals.

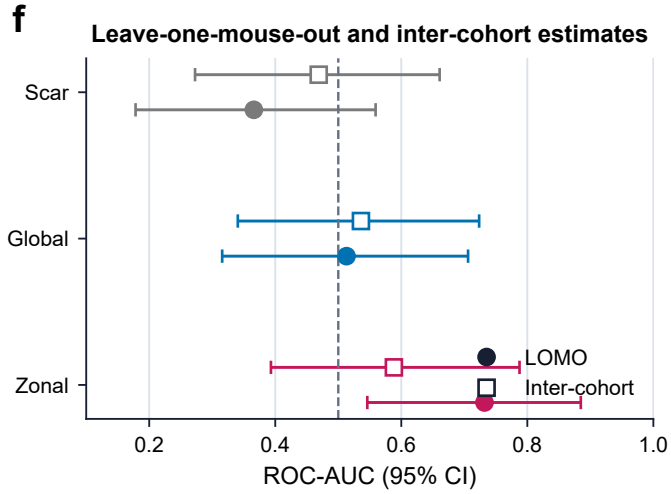












g

Primary model	35 mice; regional D5 summaries; nested leave-one-mouse-out ROC-AUC 0.732
Direct contrast	Regional minus global AUC 0.219; paired P = 0.064
Transportability	Inter-cohort validation is reported separately and does not replace mouse-level validation
Continuous endpoint	Association with fibrotic-sector fraction: ρ = 0.351; full-pipeline P = 0.105

Supplementary Figure S3 | Complementary analyses and sensitivity of summarized mechanical models.

a, Selection frequency of the 15 most recurrent descriptors in the border-zone regional prediction pipeline. Bars count the outer held-out-mouse folds selecting each descriptor (maximum 35); M1-M15 are display identifiers, with full descriptor names in the source table. These are regional-task descriptors, not the selected predictors of the primary mouse-level burden model.

b, Exploratory regional-task ROC-AUC at D0, D5 and D30, using all available eligible mice at each acquisition time without performance-based exclusions. Points and error bars show the mean and sample standard deviation across two algorithms, L2-penalized logistic regression and linear support-vector classification. These bars describe variation between algorithms, not confidence intervals or between-mouse variability. Each algorithm used held-out-mouse validation.

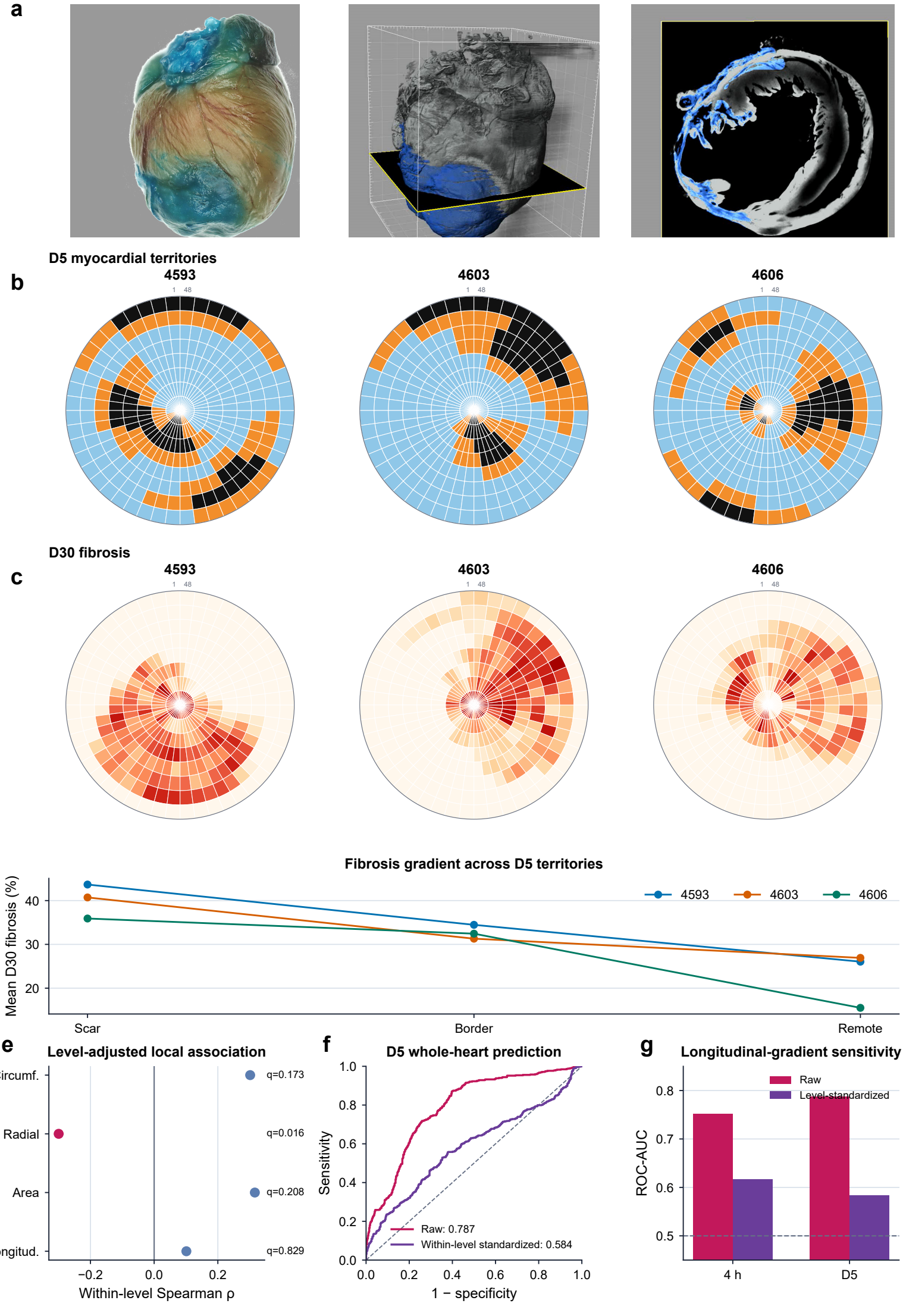
c, Exploratory mouse-level incremental-value comparisons in the same 35 mice. Reference models combined D5 mechanically defined scar fraction and ejection fraction (EF) with global circumferential strain (GCS), global longitudinal strain (GLS), or mean radial cycle area; paired bars show observed out-of-fold ROC-AUC before and after adding the cross-fitted regional-mechanics score. No uncertainty bars are shown.

d, Full-pipeline spatial perturbation analyses: 199 circular shifts and 99 unrestricted sector permutations within mice, moving complete regional descriptor vectors relative to the fixed D5 territory map. The mouse outcome and scar fraction were retained, and nested model development was repeated after each perturbation. The vertical line marks observed ROC-AUC (0.732). One-sided permutation P values were 0.100 and 0.130, respectively, using the plus-one correction.

e, Associations with continuous fibrosis outcomes. Sector fraction is the proportion of fibrotic sectors outside scar; mean histology is the mean continuous fibrosis percentage outside scar. The final row is the difference between the regional-score and global-score Spearman correlations with sector fraction, not the correlation of a score difference with fibrosis. Error bars, where available, are percentile 95% intervals from 10,000 paired mouse bootstrap resamples of fixed out-of-fold scores; points without error bars have no interval estimated in the source analysis.

f, Mouse-level ROC-AUC for scar-only, global and regional models under leave-one-mouse-out (filled circles) and leave-one-cohort-out validation (open squares). Bars are percentile 95% intervals from 2,000 mouse bootstrap resamples of fixed predictions. The global and regional models both contain mandatory scar fraction; global summaries comprise sector means and standard deviations. These intervals do not repeat model development.

g, Summary of primary and complementary findings. The continuous-outcome full-pipeline P value (0.105) is one-sided, based on 199 outcome permutations with complete nested refitting. All primary mouse-level comparisons retain the 35 mice; sensitivity analyses do not replace independent validation.


a
D5 myocardial territories
b
4593
4603
4606
1 48
D30 fibrosis
c
d
Fibrosis gradient across D5 territories
Mean D30 fibrosis (%)
40
30
20
4593
4603
4606
Scar
Border
Remote
e
Level-adjusted local association
Circumf.
Radial
Area
Longitud.
q=0.173
q=0.016
q=0.208
q=0.829
−0.2
0.0
0.2
Within-level Spearman ρ
f
D5 whole-heart prediction
Sensitivity
1 − specificity
Raw: 0.787
Within-level standardized: 0.584
g
Longitudinal-gradient sensitivity
ROC-AUC
Raw
Level-standardized
4 h
D5

Supplementary Figure S4 | Whole-heart fibrosis imaging and spatial-resolution sensitivity analysis.

a, Representative heart stained en bloc with Alcian blue (left), high-resolution episcopic microscopy (HREM) volume with a sectioning plane (middle), and the corresponding section with fibrosis segmentation (right). These supplied images illustrate whole-organ localization and extraction of fibrosis measurements.

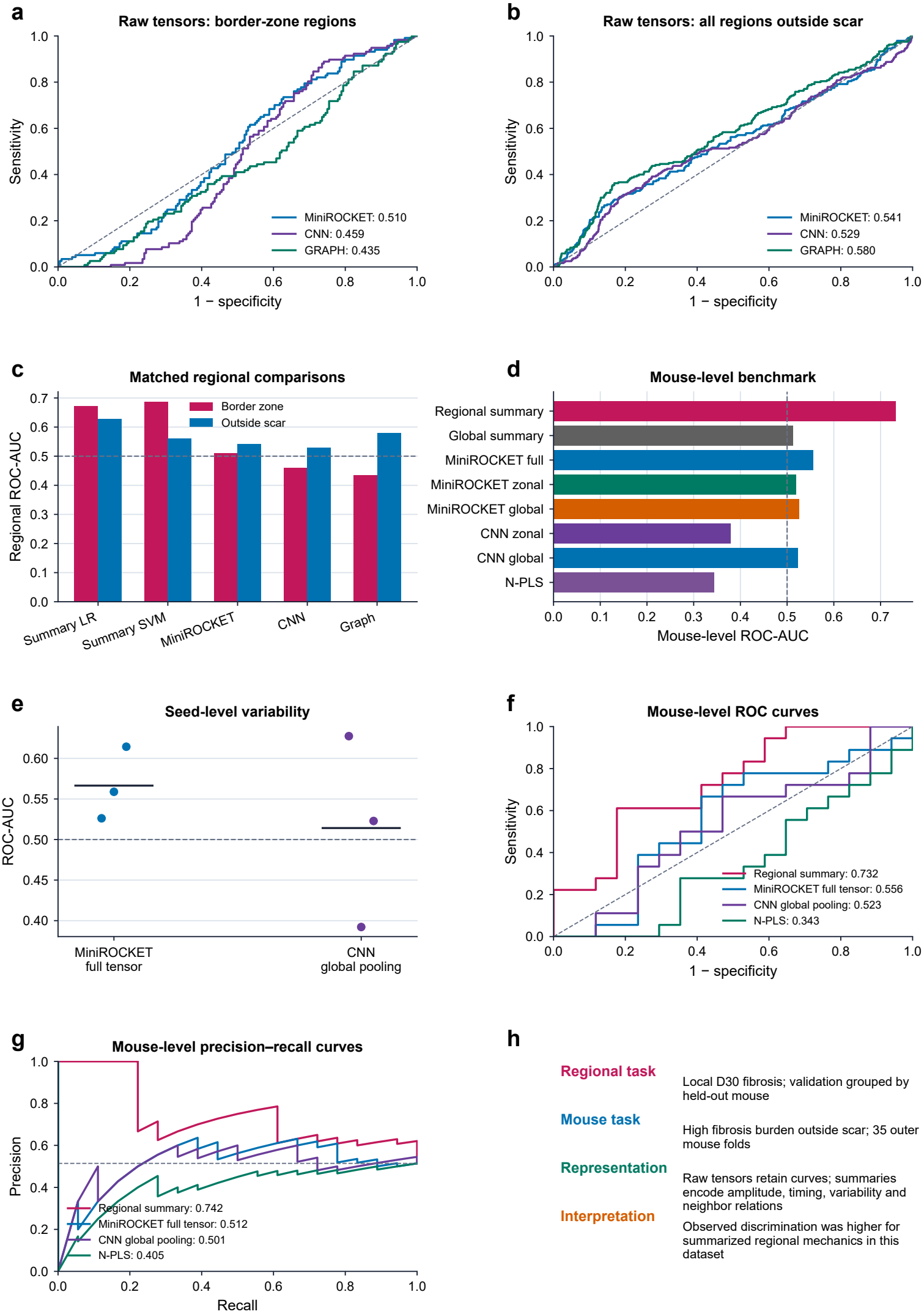
b,c, D5 mechanically defined territories (b) and D30 fibrosis percentage (c) across eight longitudinal levels and 48 circumferential sectors in each of three hearts (384 spatial cells per heart). Level 0.48 mm is central and level 3.84 mm peripheral, without a central hole. Sector 1 is immediately left of the upper reference axis and sector 48 immediately right; numbering progresses counterclockwise.

d, Mean continuous D30 fibrosis percentage within each D5 territory for each heart. Connected points represent the same heart across scar, border and remote territories; no uncertainty intervals are shown.

e, Mean within-level Spearman association between D5 mechanics and fibrosis for four strain metrics. Associations were calculated per heart after removing longitudinal-level effects and combined with equal heart weights. Two-sided spatial tests used 999 within-heart circular shifts; Benjamini-Hochberg q values were adjusted over all 16 D5 comparisons (four metrics by four scopes: all cells, scar, border and remote), not only the four displayed metrics. No confidence intervals are shown.

f, Pooled held-out-heart ROC curves for ridge models using four raw strain metrics or those metrics standardized within each heart and longitudinal level. Predictions concern binary fibrosis in border and remote cells, using the same strict >10% whole-wall fibrosis criterion. Each of the three hearts was held out in turn.

g, Corresponding ROC-AUC values at 4 h and D5; bars are point estimates without uncertainty intervals. The three hearts, not the individual spatial cells, are the independent biological units. These analyses assess spatial resolution and longitudinal gradients, rather than providing independent validation; level standardization evaluates how much discrimination remains beyond those gradients.


a
Raw tensors: border-zone regions
Sensitivity
1 − specificity
MiniROCKET: 0.510
CNN: 0.459
GRAPH: 0.435
b
Raw tensors: all regions outside scar
Sensitivity
1 − specificity
MiniROCKET: 0.541
CNN: 0.529
GRAPH: 0.580
c
Matched regional comparisons
Regional ROC-AUC
Border zone
Outside scar
Summary LR
Summary SVM
MiniROCKET
CNN
Graph
d
Mouse-level benchmark
Regional summary
Global summary
MiniROCKET full
MiniROCKET zonal
MiniROCKET global
CNN zonal
CNN global
N-PLS
Mouse-level ROC-AUC
e
Seed-level variability
ROC-AUC
MiniROCKET full tensor
CNN global pooling
f
Mouse-level ROC curves
Sensitivity
1 − specificity
Regional summary: 0.732
MiniROCKET full tensor: 0.556
CNN global pooling: 0.523
N-PLS: 0.343
g
Mouse-level precision–recall curves
Precision
Recall
Regional summary: 0.742
MiniROCKET full tensor: 0.512
CNN global pooling: 0.501
N-PLS: 0.405
h
Regional task
Local D30 fibrosis; validation grouped by held-out mouse
Mouse task
High fibrosis burden outside scar; 35 outer mouse folds
Representation
Raw tensors retain curves; summaries encode amplitude, timing, variability and neighbor relations
Interpretation
Observed discrimination was higher for summarized regional mechanics in this dataset

Supplementary Figure S5 | Detailed performance of models fitted directly to deformation signals.

a,b, Held-out-mouse ROC curves for MiniROCKET, convolutional neural-network (CNN) and graph models using raw D5 deformation tensors to classify regional D30 fibrosis in border-zone sectors (a; 321 sectors) or all sectors outside scar (b; 1,481 sectors). A fibrotic sector had strictly >10% whole-wall fibrosis. All 35 primary mice were retained, with every sector from the held-out mouse excluded from model development.

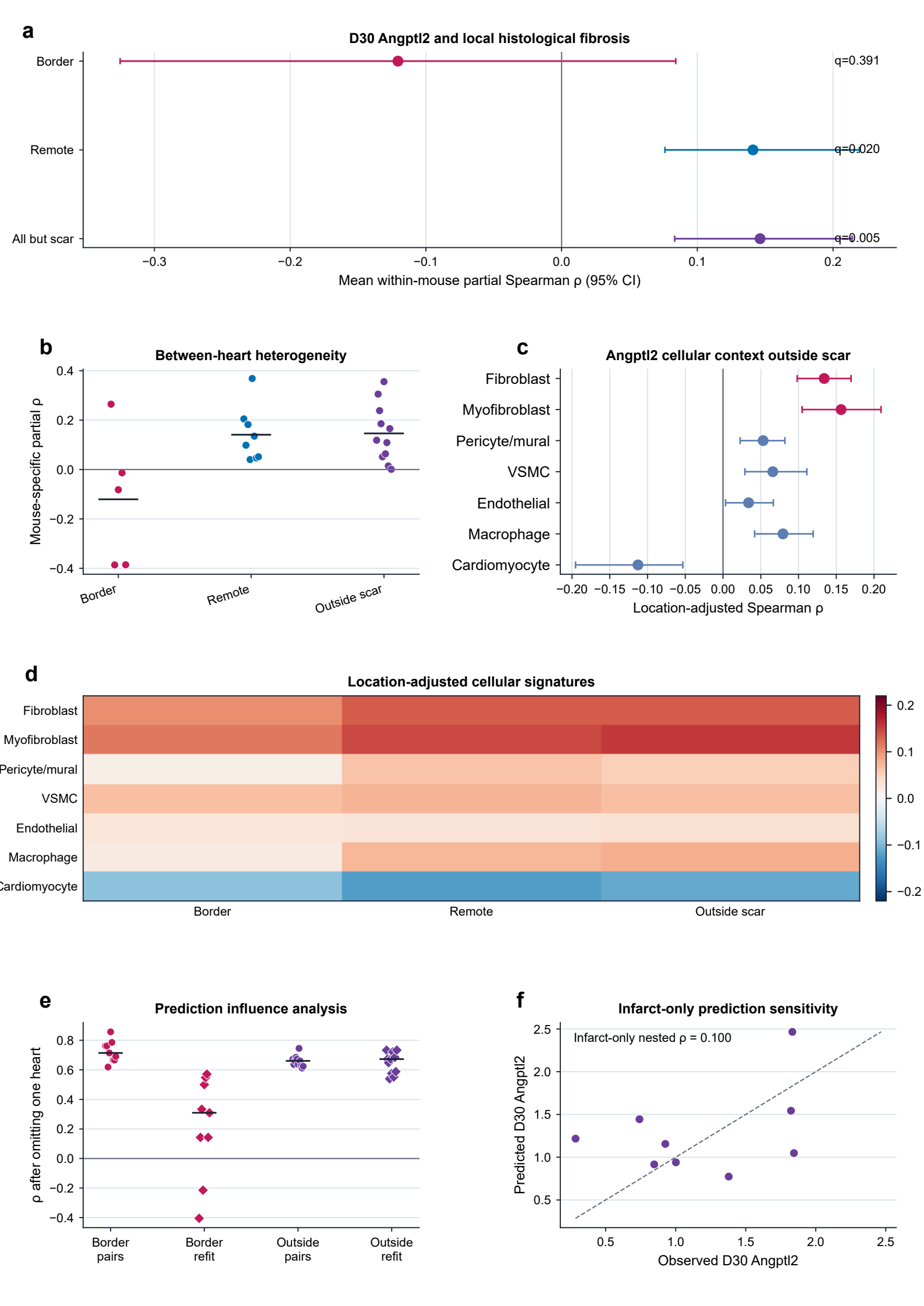
c, Matched regional-task ROC-AUC comparison with logistic-regression (LR) and linear support-vector (SVM) models using summarized mechanics. Within each territory, models used the same mice, eligible sectors, outcomes and outer held-out-mouse partitions. Bars are point estimates, not uncertainty intervals.

d, Mouse-level ROC-AUC for summarized regional and global representations and direct models using complete tensors, territory-averaged curves or globally averaged curves. The outcome was high fibrosis burden outside scar, defined at or above the cohort median (18 high-burden and 17 lower-burden mice); the common cutoff was not recalculated within folds. Both summarized models contain scar fraction as a mandatory covariate; global summaries comprise sector means and standard deviations. N-way partial least squares (N-PLS) was added post hoc.

e, Variation across three random seeds (11, 29 and 47) for the complete-tensor MiniROCKET model and globally pooled CNN. Each point is one seed's out-of-fold ROC-AUC; short horizontal lines mark arithmetic means across seeds, not confidence intervals.

f,g, Mouse-level ROC and precision-recall curves for selected models. MiniROCKET and CNN curves use predictions averaged across the three seeds; their ensemble AUC need not equal the mean seed-level AUC in e. Precision-recall area is calculated by trapezoidal integration, not average precision. Dashed lines mark the ROC chance diagonal and the positive-class prevalence for precision-recall (18/35), respectively. No confidence bands are shown.

h, Distinction between regional localization and mouse-level burden prediction. All mouse-level results use the same 35 outer leave-one-mouse-out partitions, without post-hoc performance-based exclusions. These are internal representation comparisons within this experimental cohort.


a
D30 Angptl2 and local histological fibrosis
Border
Remote
All but scar
q=0.391
q=0.020
q=0.005
−0.3
−0.2
−0.1
0.0
0.1
0.2
Mean within-mouse partial Spearman ρ (95% CI)
b
Between-heart heterogeneity
Mouse-specific partial ρ
0.4
0.2
0.0
−0.2
−0.4
Border
Remote
Outside scar
c
Angptl2 cellular context outside scar
Fibroblast
Myofibroblast
Pericyte/mural
VSMC
Endothelial
Macrophage
Cardiomyocyte
−0.20 −0.15 −0.10 −0.05 0.00 0.05 0.10 0.15 0.20
Location-adjusted Spearman ρ
d
Location-adjusted cellular signatures
Fibroblast
Myofibroblast
Pericyte/mural
VSMC
Endothelial
Macrophage
Cardiomyocyte
Border
Remote
Outside scar
0.2
0.1
0.0
−0.1
−0.2
e
Prediction influence analysis
ρ after omitting one heart
0.8
0.6
0.4
0.2
0.0
−0.2
−0.4
Border pairs
Border refit
Outside pairs
Outside refit
f
Infarct-only prediction sensitivity
Infarct-only nested ρ = 0.100
Predicted D30 Angptl2
2.5
2.0
1.5
1.0
0.5
0.5
1.0
1.5
2.0
2.5
Observed D30 Angptl2

Supplementary Figure S6 | Exploratory Angptl2-fibrosis associations, cellular context and prediction sensitivity.

a, Association of D30 Angptl2 expression with local histological fibrosis. Within-heart partial Spearman correlations account for transmural layer and, in composite territories, myocardial zone. Points show equally weighted mean heart-specific coefficients; bars are percentile 95% intervals from 20,000 heart bootstrap resamples. Valid coefficients were available from five hearts in border, eight in remote and 11 outside scar. Two-sided exact sign-flip tests were adjusted by Benjamini-Hochberg across all five analyzed scopes (all myocardium, scar, border, remote and outside scar), not only the three shown.

b, Heart-specific coefficients underlying a; each point represents one heart and short horizontal lines their arithmetic means. No uncertainty intervals are shown.

c, Location-adjusted Angptl2 associations with seven cellular-state signatures outside scar. Points indicate the mean within-heart adjusted Spearman coefficient and bars percentile 95% intervals from 5,000 heart bootstrap resamples (11 hearts).

d, Mean adjusted coefficients for these signatures in border, remote and outside scar (9, 9 and 11 hearts, respectively). The seven displayed signatures are a subset of the 12-signature analysis family; corresponding sign-flip tests were BH-adjusted across all 12 signatures within each territory. Transmural layer was accounted for within territories, with myocardial zone additionally accounted for in the composite outside-scar analysis.

e, Leave-one-heart influence on mechanics-based Angptl2 prediction, assessed by dropping one archived out-of-fold observed/predicted pair without refitting (circles), or removing one heart and rebuilding the complete nested procedure (diamonds). Each point is one omission; horizontal lines show medians across omissions, not confidence intervals. The two procedures distinguish sensitivity of fixed predictions from sensitivity of model development.

f, Nested held-out-heart prediction rebuilt in the nine infarcted hearts only for myocardium outside scar; each point is one heart. The dashed line is identity (Spearman rho = 0.100, two-sided P = 0.798). The full series comprises nine infarcted and two sham hearts; the outside-scar analyses include both sham hearts. Spatial spots contain mixed cell populations. These exploratory follow-up analyses use the same heart series as the candidate screen and provide biological context, not independent validation or evidence of causal mediation.